Hybrid breathers in nonlinear $\mathcal{PT}$-symmetric metamaterials

Sascha Böhrkircher,[1,*] Sebastian Erfort,[1] Holger Cartarius,[1,2] and Günter Wunner[1]
[1]*Institut für Theoretische Physik 1, Universität Stuttgart, 70550 Stuttgart, Germany*
[2]*Physik und ihre Didaktik, 5. Physikalisches Institut, Universität Stuttgart, 70550 Stuttgart, Germany*

(Received 30 April 2019; published 16 December 2019)

On a two-dimensional planar parity-time-($\mathcal{PT}$-)symmetric nonlinear magnetic metamaterial, consisting of split-ring dimers with balanced gain and loss, discrete breather solutions can be found. We extend these studies and by numerical calculations reveal the existence of further stable, long-lived oscillations, with certain frequencies, in the breather spectrum. We describe these oscillations in terms of an analytical breather theory, and show that they can be interpreted as superpositions of a breather oscillation and a plane wave. We coin the term "hybrid breather" solutions for these solutions.

DOI: 10.1103/PhysRevA.100.063826

I. INTRODUCTION

Metamaterials are artificially created lattice structures which can exhibit nonintuitive properties, such as negative refractive indices or unidirectional transparency [1–6]. They can be described by multiple electronic circuits, the so-called split-ring resonators which are coupled electromagnetically to each other [7–9]. The properties of these metamaterials can be tuned by varying the dielectric material in the different split-ring resonators of the lattice or spacings between the resonators [10]. Due to the possibility of custom tailoring the basic properties of metamaterials, they can even be used to realize discrete parity-time-($\mathcal{PT}$)-symmetric nonlinear metamaterials with balanced gain and loss [11,12].

The concept of $\mathcal{PT}$ symmetry was introduced two decades ago [13] and ever since has attracted increasing attention, both theoretically and experimentally (see, e.g., the recent book by Bender [14] and references therein). $\mathcal{PT}$ symmetry has been realized experimentally, e.g., in optics [15].

Every material unavoidably has loss. However, with a compensating equal amount of gain stationary behavior still can be maintained, and thus balanced gain and loss is a very common possibility to realize $\mathcal{PT}$ symmetry.

In systems governed by nonlinear wave equations highly localized and stable oscillations, so-called breather solutions, have been found. Examples are the Akhmediev breather as a solution of the Gross-Piteavskii equation [16], the Kuznetsov-Ma breather as a solution of the sine-Gordon equation [17], or discrete breathers on nonlinear lattices [18,19]. These breather solutions represent states of excitation that can only occur in nonlinear systems. Among other things they allow for the observation of different properties of the materials [20], which is a useful application of breather oscillations. On discrete lattices breather oscillations are usually referred to as discrete breathers, or intrinsic localized modes. They have been investigated on a variety of lattices [18,19,21], and, in particular, in a one-dimensional $\mathcal{PT}$-symmetric nonlinear metamaterial [12].

The purpose of this work is to extend these studies to *two-dimensional* $\mathcal{PT}$-symmetric nonlinear metasurfaces with balanced gain and loss. By numerically solving the equations governing the planar array of coupled split-ring resonators we find another type of localized oscillations, which we call hybrid breather oscillations. In Sec. II we set up the equations of the $\mathcal{PT}$-symmetric two-dimensional metamaterial system and solve these numerically. We demonstrate that both breather and hybrid breather solutions exist in this system. In Sec. III we present an analytical model which helps to explain the appearance of hybrid breather solutions. These turn out to be superpositions of breathers and plane waves, in such a way that they are localized in one dimension and are extended in the other dimension. A short summary will be given in Sec. IV.

II. SYSTEM AND NUMERICAL RESULTS

We consider a two-dimensional array of dimers, each comprising two nonlinear split-ring resonators, one with loss and the other with an equal amount of gain (Fig. 1). Evidently this is the two-dimensional extension of the one-dimensional chain discussed in Ref. [12]. As in that reference, the split-ring resonators are coupled magnetically through dipole-dipole forces, and are regarded as *RLC* circuits. The split-ring resonators are arranged in an alternating fashion on the two-dimensional lattice, in such a way that each split-ring resonator with absorption (loss) is only surrounded by split-ring resonators with amplification (gain), and vice versa. Within each dimer, the split-ring resonators are coupled via λ_M, and the coupling between neighboring dimers is given by λ'_M in the horizontal and by $\hat{\lambda}_M$ in the vertical direction. Without loss of generality we choose $|\lambda_M| > |\lambda'_M|$. Note that the electrical coupling between the split-ring resonators can be neglected due to the relative orientations of the different split-ring resonators [8]. No external driving voltage is applied to the metamaterial.

*sascha.boehrkircher@itp1.uni-stuttgart.de

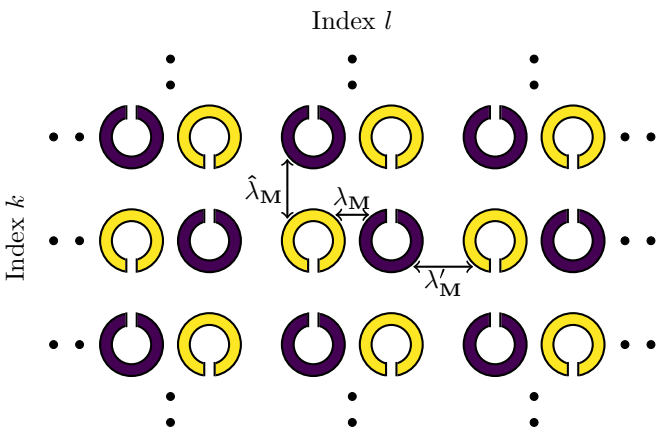

FIG. 1. Nonlinear magnetically coupled metasurface with balanced gain and loss, described by Eq. (1). Purple (dark) and yellow (bright): split-ring resonators with loss or gain, respectively.

The equations of motion for the dynamics of the charge $q_{l,k}$ in the capacitor at lattice site (l,k) can be derived in analogy with the one-dimensional case [12]. The starting point is the equivalent circuit model picture, where nearest-neighbor couplings as marked in Fig. 1 are taken into account. A detailed derivation of the one-dimensional case can be found in Ref. [10]. In addition to this case the couplings via the constants $\hat{\lambda}_M$ are added in the two-dimensional plane. This results in the coupled differential equations

$$\begin{aligned}
&\lambda'_M\ddot{q}_{2l,2k+1} + \hat{\lambda}_M\ddot{q}_{2l+1,2k} + \ddot{q}_{2l+1,2k+1} \\
&\quad +\lambda_M\ddot{q}_{2l+2,2k+1} + \hat{\lambda}_M\ddot{q}_{2l+1,2k+2} + q_{2l+1,2k+1} \\
&\quad +F(q_{2l+1,2k+1}) + \gamma\dot{q}_{2l+1,2k+1} = 0, \qquad (1a)\\
&\lambda_M\ddot{q}_{2l-1,2k+1} + \hat{\lambda}_M\ddot{q}_{2l,2k} + \ddot{q}_{2l,2k+1} \\
&\quad +\lambda'_M\ddot{q}_{2l+1,2k+1} + \hat{\lambda}_M\ddot{q}_{2l,2k+2} + q_{2l,2k+1} \\
&\quad +F(q_{2l,2k+1}) - \gamma\dot{q}_{2l,2k+1} = 0, \qquad (1b)\\
&\lambda'_M\ddot{q}_{2l,2k} + \hat{\lambda}_M\ddot{q}_{2l+1,2k-1} + \ddot{q}_{2l+1,2k} \\
&\quad +\lambda_M\ddot{q}_{2l+2,2k} + \hat{\lambda}_M\ddot{q}_{2l+1,2k+1} + q_{2l+1,2k} \\
&\quad +F(q_{2l+1,2k}) - \gamma\dot{q}_{2l+1,2k} = 0, \qquad (1c)\\
&\lambda_M\ddot{q}_{2l-1,2k} + \hat{\lambda}_M\ddot{q}_{2l,2k-1} + \ddot{q}_{2l,2k} \\
&\quad +\lambda'_M\ddot{q}_{2l+1,2k} + \hat{\lambda}_M\ddot{q}_{2l,2k+1} + q_{2l,2k} \\
&\quad +F(q_{2l,2k}) + \gamma\dot{q}_{2l,2k} = 0 \qquad (1d)
\end{aligned}$$

for each site in a 2×2 unit cell. Here, $l \in \mathbb{N}$ counts the resonators in the horizontal metachains (rows) and $k \in \mathbb{N}$ in the vertical metachains (columns). The quantity γ is the gain and loss parameter for the individual split-ring resonators and the function F describes the nonlinearity. We work in dimensionless units. The equations are normalized to the eigenfrequency of one linear split-ring resonator.

Amplification can be realized by an injection of energy through a tunneling (Esaki) diode [22], which features a negative ohmic resistance. The nonlinearity of each individual split-ring resonator can be realized by a nonlinear dielectric which is introduced into the capacitance of each split-ring resonator. For the numerical calculations a typical nonlinearity for a diode is chosen, $F(q_{x,y}) = \alpha q_{x,y}^2 + \beta q_{x,y}^3$ with $\alpha = -0.4$, $\beta = 0.08$ [20]. As the gain and loss can influence the stability of the nonlinear system [23] we choose a moderate, but yet significantly different from zero, value of $\gamma = \pm 0.002$.

Note that, because of the different couplings λ_M and $\hat{\lambda}_M$, the array is not fully $\mathcal{PT}$ symmetric in two dimensions, but only along each row and along each column. Thus the parity operator can be represented either by the spatial reflection at the center of a row *or* of a column. In both cases the time reversal operator is given by a complex conjugation. This is an example of different $\mathcal{PT}$ symmetries in two dimensions, as discussed, e.g., in Ref. [24] for a non-Hermitian XXZ spin chain. The solutions of the two-dimensional split ring array have to obey both $\mathcal{PT}$ symmetries to ensure balanced gain and loss.

Equations (1) are solved numerically by setting $q_{l,k} \propto \exp[i(l\kappa_l + k\kappa_k - \Omega\tau)]$ (with four different constants of proportionality), assuming a $1/\cosh$-type initial charge distribution around the central row, and performing a root search.

We find two-dimensional nonlinear localized, stable breather solutions. An example with frequency $\Omega_b = 0.8666$ is shown in Fig. 2. Figure 2(a) shows the breather profile, which is strongly localized in the center of the metamaterial and exponentially decaying towards its borders. The energy distribution of the central column $k = 8$, depicted in Fig. 2(b), and the energy of the central row $l = 15$, Fig. 2(c), clearly exhibit the oscillating behavior of the central split-ring resonators over 30 periods of the solution. It can be seen that in both cases the energy oscillates in a stable fashion and does not disperse along either the central column or the central row.

While numerically calculating breather solutions on this metamaterial (1), we also detected other types of solutions such as the one shown in Fig. 3.

Here, a sinusoidal initial charge distribution in the k direction and a localized shape around the middle of the l direction was chosen. We find again a breather type oscillation of the central column $k = 8$, Fig. 3(b), but, on the other hand, several oscillations around the central row $l = 15$, Fig. 3(c). It can be seen that in both cases the energy oscillates in a stable manner, with no dispersion of the energy distributions. The stability of this type of solution corresponds to that of the two-dimensional breather solution shown in Fig. 2.

These oscillations have strong resemblance to a breather solution; however, it is definitely not a two-dimensional breather. To understand the behavior of this special type of breather oscillation, which we call hybrid breather, we will consider an analytical model which starts from the superposition of a breather solution and a plane wave solution in the next section.

III. ANALYTICAL RESULTS

The breather spectrum of a system can be calculated analytically with the usual approximation of dividing the breather oscillation into two major parts [18], the nonlinear central part, also called the breather core, and the linearized part at the borders, called breather tails. At the borders the linearized coupled differential equations of the system are solved with the breather tails ansatz. This separation approximation for the analytical breather solution can be chosen because we are looking for spatially decaying solutions on a lattice, which

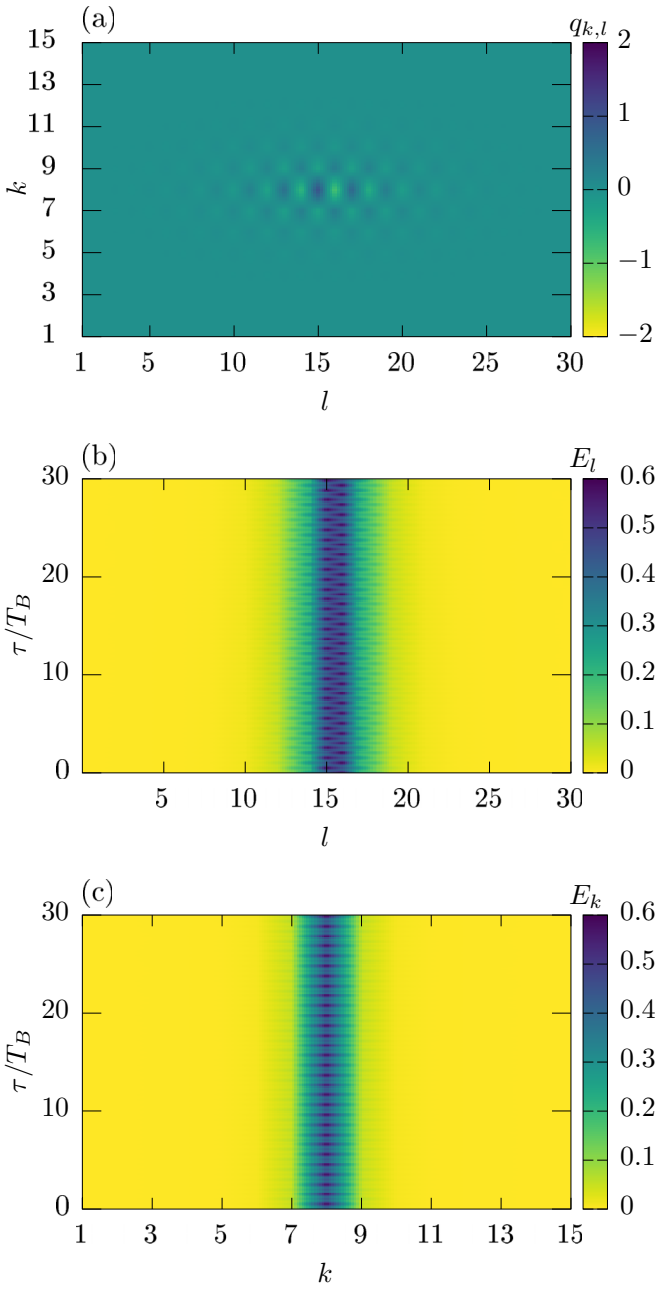

FIG. 2. Breather solution with a frequency $\Omega_b = 0.8666$ for a system with $k = 1 \ldots 15$, $l = 1 \ldots 30$, $\lambda_M = -0.17$, $\lambda'_M = -0.1$, $\hat{\lambda}_M = -0.015$, and $\gamma = \pm 0.002$, (a) breather profile of the system, (b) energy of the central column, and (c) energy of the central row in multiples of the breather period T_B.

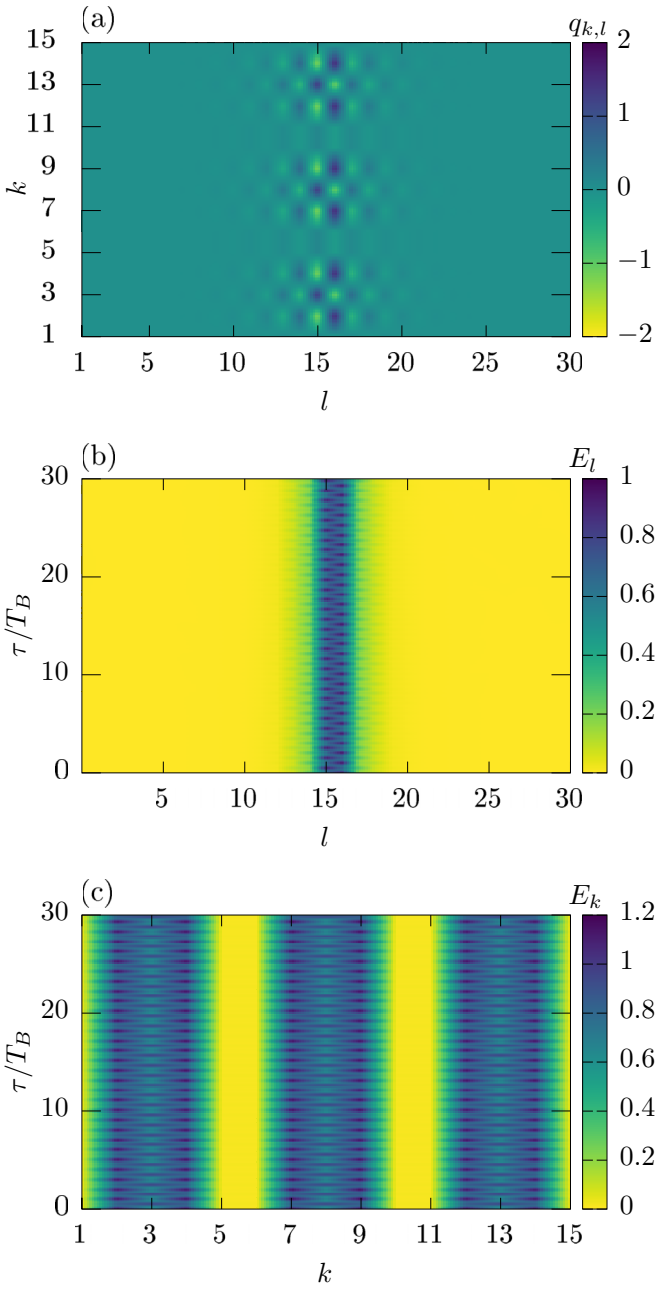

FIG. 3. Hybrid breather solution, with breather part along the l direction, (a) breather profile of the system, (b) energy of the central column, and (c) energy of the central row in multiples of the breather period T_B for a system with $k = 1 \ldots 15$, $l = 1 \ldots 30$, $\lambda_M = -0.17$, $\lambda'_M = -0.1$, $\hat{\lambda}_M = -0.015$, and $\gamma = \pm 0.002$.

have the characteristic that after a certain lattice site the amplitude of the on-site oscillations is small enough to neglect the nonlinear interactions.

To obtain the spectrum of a hybrid breather solution an ansatz

$$\begin{aligned} q_{2x,2y+1} &= A\, e^{2x\kappa_X + i[(2y+1)\kappa_Y - \Omega\tau]}, \\ q_{2x+1,2y+1} &= B\, e^{(2x+1)\kappa_X + i[(2y+1)\kappa_Y - \Omega\tau]}, \\ q_{2x,2y} &= C\, e^{2x\kappa_X + i(2y\kappa_Y - \Omega\tau)}, \\ q_{2x+1,2y} &= D\, e^{(2x+1)\kappa_X + i(2y\kappa_Y - \Omega\tau)}, \end{aligned} \tag{2}$$

with the normalized wave vectors $\kappa_{X,Y} \in \mathbb{R}$, is inserted into the linearized coupled differential equations of the system (1), which is similar to a main breather frequency ansatz in one dimension denoted by X and a plane wave ansatz in the other dimension called Y. The arbitrary coordinates X and Y for the hybrid breather solution are chosen to show the independence of the existence of hybrid breather solutions from the direction of the breather or the plane wave part.

By requiring nontrivial solutions for the resulting stationary problem one obtains

$$\Omega_{\gamma;\pm} = \Omega^4(\sqrt{\lambda_\mu} \pm \hat{\mu}_k)^2, \tag{3}$$

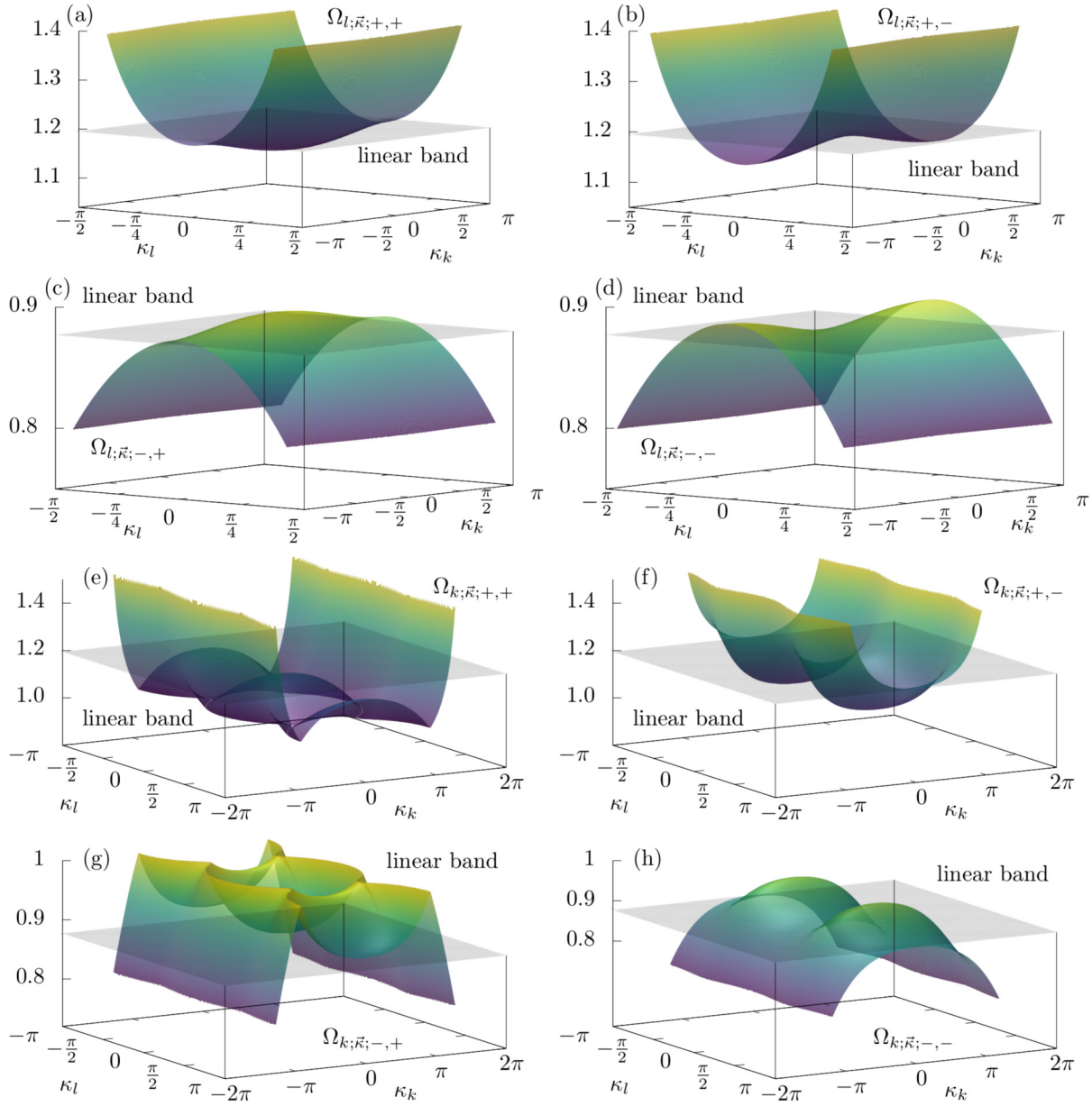

FIG. 4. Analytically approximated hybrid breather solutions obtained with Eq. (4) for coupling constants $\lambda_M = -0.17$, $\lambda'_M = -0.1$, and $\hat{\lambda}_M = -0.015$, (a) $\Omega_{l;\vec{\kappa};+,+}$, (b) $\Omega_{l;\vec{\kappa};+,-}$, (c) $\Omega_{l;\vec{\kappa};-,+}$, (d) $\Omega_{l;\vec{\kappa};-,-}$ with a breather shape along the dimer chains in l direction, (e) $\Omega_{k;\vec{\kappa};+,+}$, (f) $\Omega_{k;\vec{\kappa};+,-}$, (g) $\Omega_{k;\vec{\kappa};-,+}$, and (h) $\Omega_{k;\vec{\kappa};-,-}$ with a breather shape orthogonal to the dimer chains in k direction. The gray planes indicate the frequency of the lower and upper edges of the allowed linear frequency band. Explicitly, the breather condition reads $\Omega < 0.8771$ or $\Omega > 1.1952$.

where $\lambda_\mu = (\lambda_M - \lambda'_M)^2 + \mu_l \mu'_l$ and $\Omega_\gamma = (1-\Omega^2)^2 + \gamma^2\Omega^2$. Solving the equation with respect to Ω yields four frequencies, and because of the $\mathcal{PT}$ symmetry just positive frequency solutions are considered,

$$\Omega_{b;\vec{\kappa};\pm,\pm} = \sqrt{\frac{1 - \frac{\gamma^2}{2} \pm \sqrt{\frac{\gamma^4}{4} - \gamma^2 + (\sqrt{\lambda_\mu} \pm \hat{\mu}_k)^2}}{[1 - (\sqrt{\lambda_\mu} \pm \hat{\mu}_k)^2]}}. \quad (4)$$

For a hybrid breather solution, with a breather shape along the dimer chains in l direction, the substituted variables are

$$\begin{aligned} \mu_l &= 2\lambda_M \cosh(\kappa_l), \quad \mu'_l = 2\lambda'_M \cosh(\kappa_l), \\ \hat{\mu}_k &= 2\hat{\lambda}_M \cos(\kappa_k), \end{aligned} \quad (5)$$

and with a breather shape orthogonal to the dimer chains in k direction

$$\begin{aligned} \mu_l &= 2\lambda_M \cos(\kappa_l), \quad \mu'_l = 2\lambda'_M \cos(\kappa_l), \\ \hat{\mu}_k &= 2\hat{\lambda}_M \cosh(\kappa_k). \end{aligned} \quad (6)$$

These four analytically calculated solutions are displayed in Fig. 4 for the same parameters as used in the numerically calculated solution (Fig. 3), and for both cases of the substituted variables given in Eqs. (5) and (6). In Figs. 4(a)–4(d) the four solutions are displayed for a breather shape along the dimer chains in l direction. It can be seen that the solutions $\Omega_{b;\vec{\kappa};+,+}$ in Fig. 4(a) and $\Omega_{b;\vec{\kappa};+,-}$ in Fig. 4(b) as well as $\Omega_{b;\vec{\kappa};-,+}$ in Fig. 4(c) and $\Omega_{b;\vec{\kappa};-,-}$ in Fig. 4(d) are similar

to each other and can be transformed into one another by a shift of $\Delta\kappa_k = \pi$. In Figs. 4(e)–4(h) the four solutions are displayed for a breather shape orthogonal to the dimer chains in k direction. With Eqs. (4) and (6) it can be seen that the solutions $\Omega_{b;\vec{\kappa};+,+}$ in Fig. 4(e) and $\Omega_{b;\vec{\kappa};+,-}$ in Fig. 4(f) as well as $\Omega_{b;\vec{\kappa};-,+}$ in Fig. 4(g) and $\Omega_{b;\vec{\kappa};-,-}$ in Fig. 4(h) are the same for $\kappa_k = 0$. A closer look at these pairs of solutions reveals that for small values of κ_k the solutions differ from each other but merge again into each other for higher values of κ_k.

To obtain a true hybrid breather solution these four solutions with the pseudo wave vector $\kappa = (\kappa_l, \kappa_k)^T$ have also to fulfill the breather condition that their frequencies must not lie in the (allowed) frequency band of plane wave solutions [21]

$$\Omega_b \neq \Omega_{\text{plane wave}}, \tag{7}$$

which is obtained by solving the linearized system equations. For the parameters considered here the lower edge of the band is found to be $\Omega = 0.8771$ and the upper edge $\Omega = 1.1952$. The breather condition (7) is requisite to guarantee the existence of a stable breather core of the hybrid breather oscillation. Out of this condition not every pseudo wave vector of all four analytically calculated solutions belongs to a frequency in the allowed domain. It can be seen in Fig. 4 that for the solutions $\Omega_{b;\vec{\kappa};+,+}$ and $\Omega_{b;\vec{\kappa};+,-}$ only hybrid breather solutions with a frequency above the upper edge of the allowed frequency band ($\Omega = 1.1952$) are found. Analogously this can be applied to $\Omega_{b;\vec{\kappa};-,+}$ and $\Omega_{b;\vec{\kappa};-,-}$, where the pseudovector needs to belong to a frequency under the lower edge of the allowed frequency band ($\Omega = 0.8771$).

For the analytical breather solution with a breather shape along the k direction two favorable solutions $\Omega_{b;\vec{\kappa};+,-}$ and $\Omega_{b;\vec{\kappa};-,-}$ exist. They have a much smaller range of pseudo wave vectors which belong to frequencies inside the linear band structure. Thus these solutions can describe true hybrid breather solutions for more pseudo wave vectors than the other two analytical solutions. On the other hand, the analytical breather solutions with a breather shape along the l direction do not have any favorable solutions, because each solution has the same amount of pseudo wave vectors belonging to frequencies inside the linear band structure.

It is interesting to note that if the analytical $\Omega_{b;\vec{\kappa};+,+}$ hybrid breather solution fulfills the breather condition for a certain pseudo wave vector κ, then also $\Omega_{b;\vec{\kappa};-,+}$ fulfills the condition for the same pseudo wave vector, and vice versa. The same can be observed for $\Omega_{b;\vec{\kappa};+,-}$ and $\Omega_{b;\vec{\kappa};-,-}$, which is shown in Fig. 4.

The analytical model was calculated using the linearization approximation for the breather tails. It covers all solutions that contain exponentially dropping tails. This is independent from the nonlinearity chosen since we only look at those parts of the tails which have an amplitude small enough for the nonlinearities to be insignificant. Therefore, this model describes every possible hybrid breather excitation caused by some nonlinearity in the breather core. However, the numerically observable hybrid breather oscillations depend strongly on the nonlinearity chosen for the system and the shape of the breather core. Analogous to the normal breather oscillations the hybrid breather oscillations have to obey $\mathcal{PT}$ symmetry to obtain long-lived oscillations. The nonlinearities chosen in this paper represent a typical diode [12].

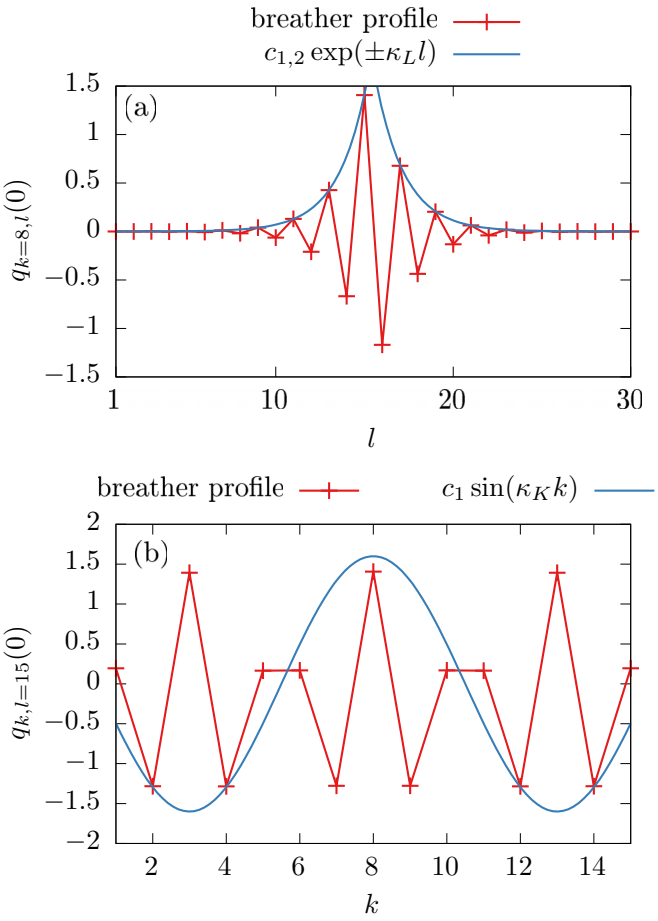

FIG. 5. Comparison between the breather profile of the numerically calculated system (Fig. 3) and the analytical model (Fig. 4) with the same coupling constants for (a) the central column (8th) and (b) the central row (15th) of the system.

The results of the analytical theory can now be compared with the numerically observed hybrid breather oscillation, shown in Fig. 3, with a standing plane wave form along the k direction. In Fig. 5(a) we compare the breather profile along the central column: the breather part for the numerically calculated hybrid breather solution (red lines with crosses) and the analytical exponential functions (blue solid lines). As can be seen in the diagram the analytical model describes the numerical values perfectly. Through this a value of $\kappa_l = 0.6$ was determined for the numerical solution. In Fig. 5(b) we compare the breather profile along the central row for the numerically calculated hybrid breather solution, the standing plane wave part (red lines with crosses) with an analytical sine function (blue solid lines). As can be seen in the diagram the sine function generally describes the numerical values quite well. Discrepancies between the numerical and the analytical solution occur because we are numerically calculating a nonlinear system with charges $|q_{k,l}(\tau/T_B)| > 1$ in which case also the nonlinearity of the split-ring resonators would have to be taken into account. This nonlinearity of the split-ring resonators was neglected in the analytical calculation due to the linearization approximation of the breather tails. From the comparison a value of $\kappa_k = \pi/5$ is deduced for the

numerical solution. Inserting the numerical parameters into Eq. (4) yields the four frequency values $\Omega_{+,+} = 1.1890$, $\Omega_{+,-} = 1.2321$, $\Omega_{-,+} = 0.8795$, and $\Omega_{-,-} = 0.8635$. By comparing these values with the numerical ones it can be seen that the frequency $\Omega_{-,-} = 0.8635$ and the numerical ones are equivalent. For this reason the analytical approximation describes the hybrid breather solutions quite well for plane wave parts slightly in the nonlinear regime.

In the analytical approximation also hybrid breather solutions with a plane wave part along the l direction and hybrid breather solutions with a plane wave part along the k direction and a frequency above the linear band structure are predicted. However, such hybrid breather solutions do not appear in the numerical calculation.

An explanation for this can be found in the analytical model. To obtain a stable breather oscillation a nonlinear breather core is needed which oscillates with the breather frequency and has an according shape to induce the oscillation in the linearized breather tails. The formulated analytical model only supports nonlinear breather cores which are similar to linear plane waves, because the nonlinear breather core excites an oscillation outside of the linear band structure which then will spatially decay in the linearized breather tails. This leads to the fact that the described analytical model can only be used for not too large nonlinear hybrid breather cores. As a consequence we cannot find hybrid breather solutions with a plane wave part along the l direction and a frequency above the linear band structure in our numerical calculations. One way to find the other solutions would be to extend our analytical model to nonlinear plane waves. Another way would be the use of a metamaterial with a different nonlinearity and other breather cores.

The breather cores that can be found strongly depend on the nonlinearity of the metamaterial. By contrast the breather tails are totally independent of the nonlinearity of the metamaterial. Therefore, it is possible that similar metamaterials with slightly differing nonlinearities can exhibit quite different breather and hybrid breather solutions. This is also the reason why we evaluated all hybrid breather solutions $\Omega_{b;\vec{\kappa};\pm,\pm}$, because for every possible hybrid breather solution there could exist a nonlinear metamaterial with an appropriate nonlinearity with which it is possible to excite this hybrid breather oscillation.

IV. SUMMARY

The main result of our work is that for $\mathcal{PT}$-symmetric nonlinear metamaterials with balanced gain and loss in dimensions $d > 1$ mixed types of breather oscillations can exist, in addition to usual breathers.

We have shown this by numerically solving the equations of motion describing the dynamics of the charges in the individual split-ring capacitors of a $\mathcal{PT}$-symmetric nonlinear metasurface. These, as we call them, "hybrid breather" solutions could be explained by an analytical model, in which the breather was divided into a nonlinear central part and a linearized outer part, and by allowing a linear plane wave shape in one direction.

[1] H.-T. Chen, W. J. Padilla, J. M. O. Zide, A. C. Gossard, A. J. Taylor, and R. D. Averitt, Nature (London) **444**, 597 (2006).

[2] N. Yu and F. Capasso, Nat. Mater. **13**, 139 (2014).

[3] R. A. Shelby, D. R. Smith, and S. Schultz, Science **292**, 77 (2001).

[4] V. M. Shalaev, Nat. Photon. **1**, 41 (2007).

[5] Z. Lin, H. Ramezani, T. Eichelkraut, T. Kottos, H. Cao, and D. N. Christodoulides, Phys. Rev. Lett. **106**, 213901 (2011).

[6] D. Schurig, J. J. Mock, B. J. Justice, S. A. Cummer, J. B. Pendry, A. F. Starr, and D. R. Smith, Science **314**, 977 (2006).

[7] O. Sydoruk, A. Radkovskaya, O. Zhuromskyy, E. Shamonina, M. Shamonin, C. J. Stevens, G. Faulkner, D. J. Edwards, and L. Solymar, Phys. Rev. B **73**, 224406 (2006).

[8] F. Hesmer, E. Tatartschuk, O. Zhuromskyy, A. A. Radkovskaya, M. Shamonin, T. Hao, C. J. Stevens, G. Faulkner, D. J. Edwards, and E. Shamonina, Phys. Status Solidi B **244**, 1170 (2007).

[9] I. Sersic, M. Frimmer, and A. F. Koenderink, Phys. Rev. Lett. **103**, 213902 (2009).

[10] N. Lazarides, M. Eleftheriou, and G. P. Tsironis, Phys. Rev. Lett. **97**, 157406 (2006).

[11] J. Schindler, A. Li, M. C. Zheng, F. M. Ellis, and T. Kottos, Phys. Rev. A **84**, 040101(R) (2011).

[12] N. Lazarides and G. P. Tsironis, Phys. Rev. Lett. **110**, 053901 (2013).

[13] C. M. Bender and S. Boettcher, Phys. Rev. Lett. **80**, 5243 (1998).

[14] C. M. Bender, *PT Symmetry in Quantum and Classical Physics* (World Scientific, Singapore, 2018).

[15] C. E. Rüter, K. G. Makris, R. El-Ganainy, D. N. Christodoulides, M. Segev, and D. Kip, Nat. Phys. **6**, 192 (2010).

[16] N. N. Akhmediev, V. M. Eleonskii, and N. E. Kulagin, Theor. Math. Phys. **72**, 809 (1987).

[17] E. Kuznetsov, Sov. Phys. Dokl. **22**, 507 (1977).

[18] M. Ohtsu and T. Yatsui, *Progress in Nanophotonics 3*, Nano-Optics and Nanophotonics (Springer International Publishing, Berlin, 2014).

[19] A. J. Sievers and S. Takeno, Phys. Rev. Lett. **61**, 970 (1988).

[20] N. Lazarides, V. Paltoglou, and G. P. Tsironis, Int. J. Bifurcat. Chaos **21**, 2147 (2011).

[21] S. Flach and A. V. Gorbach, Phys. Rep. **467**, 1 (2008).

[22] L. Esaki, Phys. Rev. **109**, 603 (1958).

[23] D. Haag, D. Dast, A. Löhle, H. Cartarius, J. Main, and G. Wunner, Phys. Rev. A **89**, 023601 (2014).

[24] O. A. Castro-Alvaredo and A. Fring, J. Phys. A **42**, 465211 (2009).